THE PUBLISHING HOUSE
OF THE ROMANIAN ACADEMY

PROCEEDINGS OF THE ROMANIAN ACADEMY, Series A,
Volume 17, Number 3/2016, pp. 222–229

PROPAGATION ROBUSTNESS OF TWO LAGUERRE-GAUSS BEAM SUPERPOSITION

Rebeca TUDOR[1, 2] Mona MIHAILESCU[3], Irina Alexandra PAUN[3], Ana Elena NAN[3], Mihai KUSKO[1], Cristian KUSKO[1]

[1] Institute for Microtechnology, Bucharest, Romania
[2] University of Bucharest, Physics Faculty, Bucharest, Romania
[3] Politehnica University of Bucharest, Bucharest, Romania
Corresponding author: Mona MIHAILESCU, E-mail: mona_m@physics.pub.ro

Abstract. We analyzed the intensity distribution resulted from the axial superposition of two Laguerre-Gauss beams. It is found that the intensity spatial distribution can be transformed from interference patterns with uniform maxima and round holes or radial petals, to one consisting of separated rings, by simply changing of the interrelations between constructive parameters. The propagation robustness of two Laguerre-Gauss beam superposition is investigated for different ranges of the constructive parameter values using experimental and simulation results. Combinations of different optical angular momentum states can be obtained, transmitted and read, with almost the same efficiency in the detection process.

Key words: Laguerre-Gauss beams, axial superposition, helical phase distribution, spatial light modulator

1. INTRODUCTION

Laser beams with specific intensity distribution along propagation axis or in planes perpendicular to the optical axis are used in applications such as: optical tweezers [1, 2], nondiffracting beams [3, 4], multidimensional modulation [5], multiple focal points along the optical axis [6] compressed femtosecond laser pulses [7], compensation of the spatial distortion in laser beams [8], optical information transfer [9], and multiple beams with equal intensities [10].

A simple method, to obtain these spatially modulated beams, is to use diffractive optical elements (DOEs) with structures computed in different ways: interference between a reference and an object beam [11], iterative Fourier transform algorithm [12], and analytical equations [13]. The diffracted intensity patterns (DIPs) from these DOEs can be obtained using spatial light modulators acting as reconfigurable DOEs, by addressing them from a computer.

One of the most studied and used phase distribution is the helical one, which is characterized by its orbital angular momentum (OAM). In this case, in DIP, a vortex beam is created. It is a manifestation of phase singularity and, consequently, it has been investigated for different applications, including optical trapping and optical information transfer [9, 14]. Optical ferris wheels were introduced [15] as a consequence of the superposition of two Laguerre-Gauss beams (LGBs) carrying two different OAM states, with applications in atoms trapping; lately, other applications appeared, e. g. multidimensional modulation [16] or multiplexing and demultiplexing multiple beams [17].

In this context, we investigated the DIPs along the propagation axis, obtained from the axial superposition of two LGBs generated with different OAM states, same initial waist and different relative intensities. The classical method of computing DOEs, by interfering the object beam with a plane wave, was employed. We show that different DIPs can be obtained depending on the chosen OAM values combination. The ranges of the constructive parameters values are discussed for each case using experimental and simulation results. Combinations of different OAM states can be obtained, transmitted and read, with almost the same efficiency in the detection process. The reading process can be performed by simple inspection in the central point of DIP, after a reading mask is introduced in the optical path.

2. GENERATION OF DIFFRACTIVE STRUCTURES

To compute the structures of the diffractive optical elements, we started with the well known analytical expression [15] that describes the LGBs. The phase has a spatial distribution $\exp(-im\theta)$, where θ is the azimuthal angle and m is the topological charge carrying a given OAM state. The scaled electric field of one LGB can be written at different distances, z, along propagation axis, as a radial distribution:

$$LG_m = A_{|m|} \exp\left[i\left(k\left(z - \frac{r^2}{2R} \right) + \Phi_{|m|} \right) \right] e^{-im\theta}, \tag{1}$$

where r is the radial coordinate. The amplitude has the following expression:

$$A_{|m|} = \sqrt{I}\sqrt{2/\left(\pi(|m|!)\right)}\left(\sqrt{2}r/w\right)^{|m|} \exp(-r^2/w^2),$$

and it is influenced by: the beam waist $w(z) = w_0\sqrt{1+(z/z_R)^2}$, (3)

the intensity parameter $I = P/w^2$, (4)

the radius of curvature $R = z\cdot\left(1+\left(z_R/z\right)^2\right)$, (5)

and the Gouy phase $\Phi_{|m|} = \left(|m|+1\right)\arctan(z/z_R)$. (6)

The propagation constant is $k = 2\pi/\lambda$, w_0 is the waist at $z = 0$, the Rayleigh distance is $z_R = \pi\cdot w_0^2/\lambda$, λ is the laser wavelength; further we will consider the laser power $P = 1$.

The orthogonal superposition of different OAM states for a communication system has already been studied [9]. Here we focus on investigating the axial superposition of two LGBs with different OAM states, but same w_0 for stability reasons, each described by Eq. (1). First, we must calculate the intensity distribution:

$$LG_{m_1,m_2} = \left| A_{|m_1|} \exp\left[i\left(k\left(z - \frac{r^2}{2R} \right) + \Phi_{|m_1|} \right) \right] e^{-im_1\theta} + A_{|m_2|} \exp\left[i\left(k\left(z - \frac{r^2}{2R} \right) + \Phi_{|m_2|} \right) \right] e^{-im_2\theta} \right|^2. \tag{7}$$

In the next step, we simulated the interference between the phase distribution of this superposition and a tilted plane wave $\exp(ik\cdot f_s\cdot x)$, where f_s is the parameter associated with the spatial frequency that determines the spatial separation in the DIP. The resulted DOEs have structures composed of a central singularity of order m_1 and a number of $\delta m = m_2 - m_1$ singularities of the first order. In the DOEs presented in the Fig. 1 different values for the basic parameters were employed.

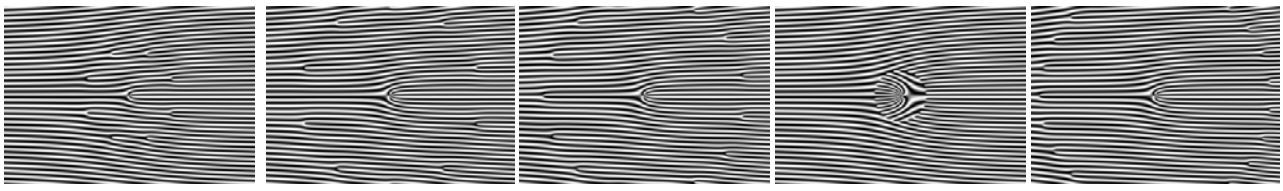

a) **b)** **c)** **d)** **e)**

Fig. 1 – DOE structures obtained as interference pattern between a plane wave and two LGBs with $z = 10$, $w_0 = 50$, $I_1 = I_2$: a) $m_1 = 3$, $m_2 = 11$; b) $m_1 = 5$, $m_2 = 15$; c) $m_1 = 5$, $m_2 = 20$; d) $m_1 = -11$, $m_2 = 11$; e) $m_1 = 5$, $m_2 = 30$ (the central parts from all DOEs were displayed).

3. PARAMETERS VARIATION ANALYSIS

For a single LGB, the intensity distribution exhibits the well-known pattern of a bright ring with a central hole of diameter proportional to the OAM value, i.e., the vortex ring. First, the behavior along the propagation axis *z*, of the waist, *w*, and intensity, *I*, in the vortex ring are analyzed in the case of a single LGB for different w_0 (Fig. 2). One can observe that the intensity decreases very rapidly for smaller values of w_0, while for larger values of w_0, the intensity is almost constant. The waist increases drastically at short distances for small values of w_0. In this case, a few relations between geometrical and intensity parameters have been demonstrated [18]:

1.1. The maximum value for intensity is $I_m / \left(4\sqrt{|m|}\right)$, at radial coordinate equal with $w\sqrt{|m|/2}$.

1.2. The electric field in the radial direction has a full width at half maximum (FWHM) of $\sqrt{2\ln(2)}w$.

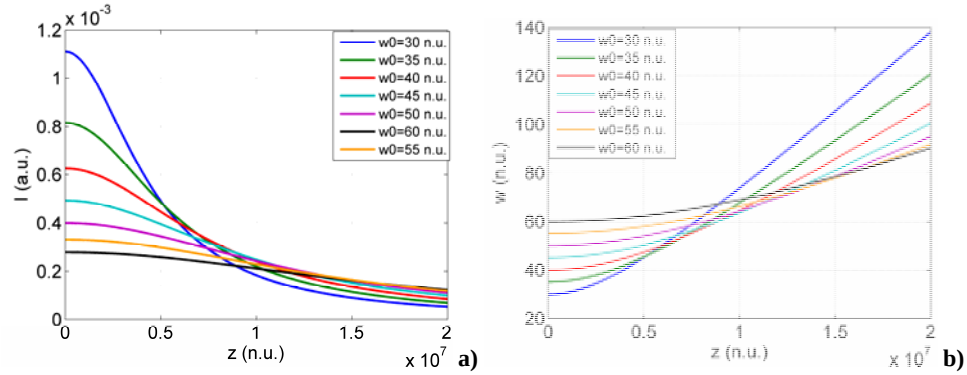

Fig. 2 – Axial behavior of the maximum intensity and the waist values at different w_0 for a single LGB.

When two LGBs are axially superposed, the condition to obtain their interference is that the position of the maximum intensities of each LGB must be spaced apart by one FWHM [15]. In this case, the DIP exhibits an approximately uniform distribution of the maxima in the cylindrically symmetric lattice (which also contains circular holes). From this, two supplementary conditions result:

2.1. The difference between their radiuses, at the point where maximum intensity is obtained for each LGB must be equal to one FWHM, which leads to $m_2 = \pm\left(\sqrt{|m_1|} + 2\sqrt{\ln(2)}\right)^2$ (Fig. 3a, blue and red curves).

2.2. $I_{m_2} = \sqrt{|m_2 / m_1|} I_{m_1}$ in order to obtain equal values for electric fields maximum intensities (Fig. 3a).

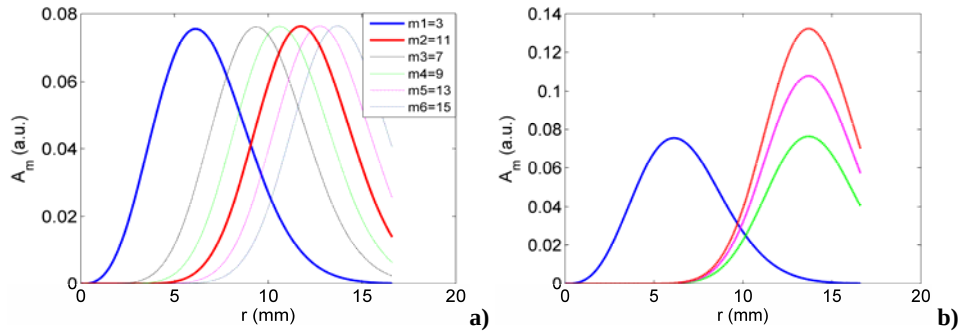

Fig. 3 – Radial distribution of the amplitude for: a) different values of OAM; b) m_1=3 and an OAM that does not fulfill the condition 2.1 (the latter computed with different values for the initial intensity).

The overlapping area of the individual intensity distribution is the most important factor that determines the characteristics of the DIPs. It varies with all the parameters and controls the presence or absence of the interference maxima and minima between the two LGBs, the relative intensity between them and can even be controlled when conditions 2.1 or 2.2 are not satisfied. If condition 2.2 is fulfilled, but condition 2.1 is not, the distances between the maxima are shorter or longer than a FWHM (Fig. 3a). This overlapping area can be modified by increasing or decreasing the intensities in one or both LGBs (Fig. 3b). For a general approach, all distance values are normalized at the pixel pitch value (in millimeters).

4. DIFFRACTED INTENSITY PATTERNS

The DOEs computed as an interference pattern, are addressed to the liquid crystal display of a spatial light modulator (LC2002, transmission mode, 0.032 mm pixel pitch). The experimental setup is the classical one containing a collimated laser beam (HeNe 632.8 nm) at normal incidence on the spatial light modulator, a CCD camera (Pike F421C 2048×2048 pixels) that records the obtained DIPs. Using adequate lens systems, our setup was prepared to acquire the far field DIPs, +1 order.

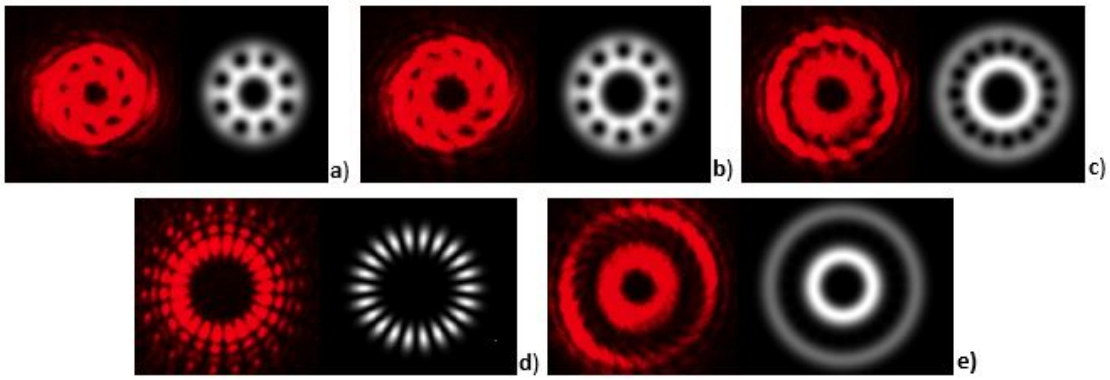

Fig. 4 – Experimental (left) and simulated (right) images of DIPs generated using DOEs computed with $w_0 = 50$, $I_1 = I_2$, at $z = 10$m: a) $m_1 = 3$, $m_2 = 11$; b) $m_1 = 5$, $m_2 = 15$; c) $m_1 = 5$, $m_2 = 20$; d) $m_1 = -11$, $m_2 = 11$; e) $m_1 = 5$, $m_2 = 30$.

For the case of equal I and w_0 for both LGBs, but different relations between m_1 and m_2, the DIPs are computed at the same z (Fig. 4, experiment and simulation). Three distinct cases of DIPs were found:

(1) Cylindrically symmetric approximately constant intensity distribution in a lattice with a number of $\delta m_h = |m_2| - |m_1|$ circular holes (Fig. 4a, b) given by the constructive interference between two LGBs, when DOEs are generated with $|m_1| \neq |m_2|$, that fulfill the condition 2.1. These DIPs are transforming when $|m_1| \neq |m_2|$, without fulfilling the condition 2.1, but with values close to the ones in the specific ratio 2.1. The number of circular holes remains $\delta m_h = |m_2| - |m_1|$ (Fig. 4c), but the intensity distribution in the radial direction becomes nonuniform (Fig. 5). The central hole diameter is constant corresponding to $m_1 = 5$.

(2) Cylindrically symmetric approximately constant intensity distribution with a number of $\delta m_p = 2|m_1|$ petals (Fig. 4d), when DOEs are generated with $|m_2| = -|m_1|$. These are transforming in a number of $\delta m_p = |m_1| + |m_2|$ petals with nonuniform radial intensities in the case when $|m_1|$ is close to $-|m_2|-$ Fig. 6. The central hole diameter is constant for $m_2 < -5$ and corresponds to $m_1 = 5$, but it decreases for $m_2 \in [-1,-4]$.

(3) Two separated rings, each corresponding to an OAM value (Fig. 4 e), if the DOEs are generated with $|m_1| \neq |m_2|$, with values far from those given by condition 2.1.

The decreasing of the maximum intensity values inside circular lattice for different m_2 values is presented in the Fig. 7 (both cases (1) and (2) are depicted).

Fig. 5 – Simulated DIPs in the case (1) for $m_1 = 5$, and m_2 equal with: a) 6; b) 7; c) 9; d) 11; e) 13; f) 15; g) 17; h) 21; i) 25.

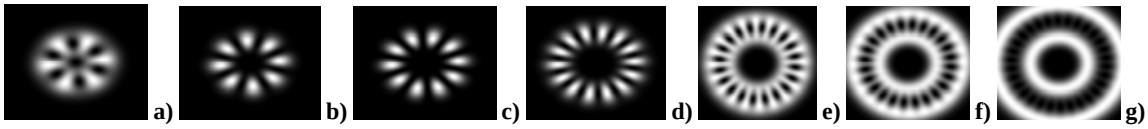

Fig. 6 – Simulated DIPs in the case (2) for $m_1 = 5$, and m_2 values equal with: a)–1; b) –3; c) –5; d) –9; e) –15; f) –19; g) –25.

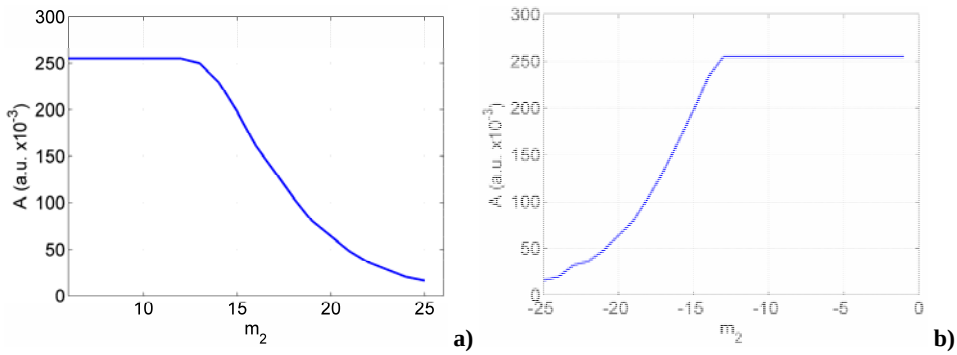

Fig. 7 – Values of the maximum intensity inside circular lattice corresponding to different m_2 values for: a) case (1) ; b) case (2).

In Fig. 8, the experimental DIPs obtained at the same z but with different initial values of the waist, w_0, are presented for all (1–3) cases (the same w_0 value for both LGBs). As it can be observed, the w_0 values have a significant influence on the DIPs except for the case of $|m_2| = -|m_1|$.

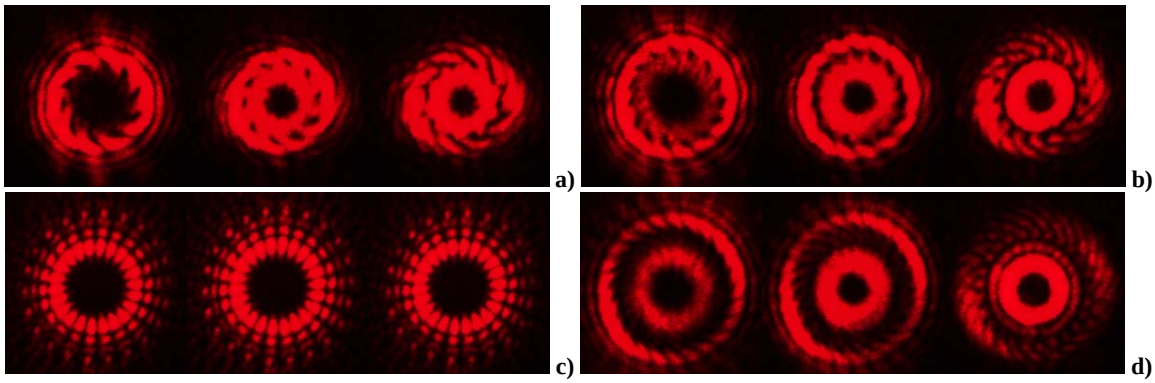

Fig. 8 – DIPs from DOEs generated with different w_0 (both LGBs use the same value for w_0: a) $m_1 = 5$, $m_2 = 15$; b) $m_1 = 5$, $m_2 = 20$; c) $m_1 = –11$, $m_2 = 11$; d) $m_1 = 5$, $m_2 = 30$. For all cases, from left to right, $w_0 = 30, 50, 70$. The intensity values are constant.

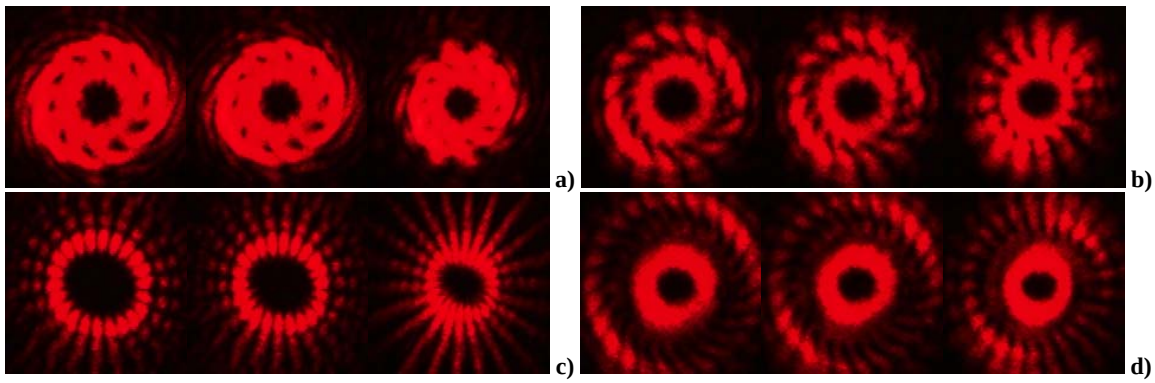

Fig. 9 – DIPs along propagation axis (both LGBs use the same value for w_0: a) $m_1 = 5$, $m_2 = 15$; b) $m_1 = 5$, $m_2 = 20$; c) $m_1 = –11$, $m_2 = 11$; d) $m_1 = 5$, $m_2 = 30$. For all cases, from left to right, $z =$ 1 m, 1 km, 5 km. The intensity values are constant.

To investigate the DIPs robustness, a study of their behavior along propagation axis is performed. In this case, of fixed given values for w_0, I, m_1 and m_2, the parameter z has a reduced influence: the DIPs are stable for z values going from a few meters to a few kilometers (see Fig. 9) in all (1–3) cases.

Condition 2.2 imposes an ideal value for $I_2 = I_{ideal}$. The results from DIPs investigation show that, in cases (1) and (3), for values in the interval $I_2 \in \left[10^{-3} \cdot I_{ideal},\ 10^{3} \cdot I_{ideal}\right]$, the diffracted intensity remains approximately unchanged (see Fig. 10) at a given z. In the case (2), the situation is different (see Fig. 10 c).

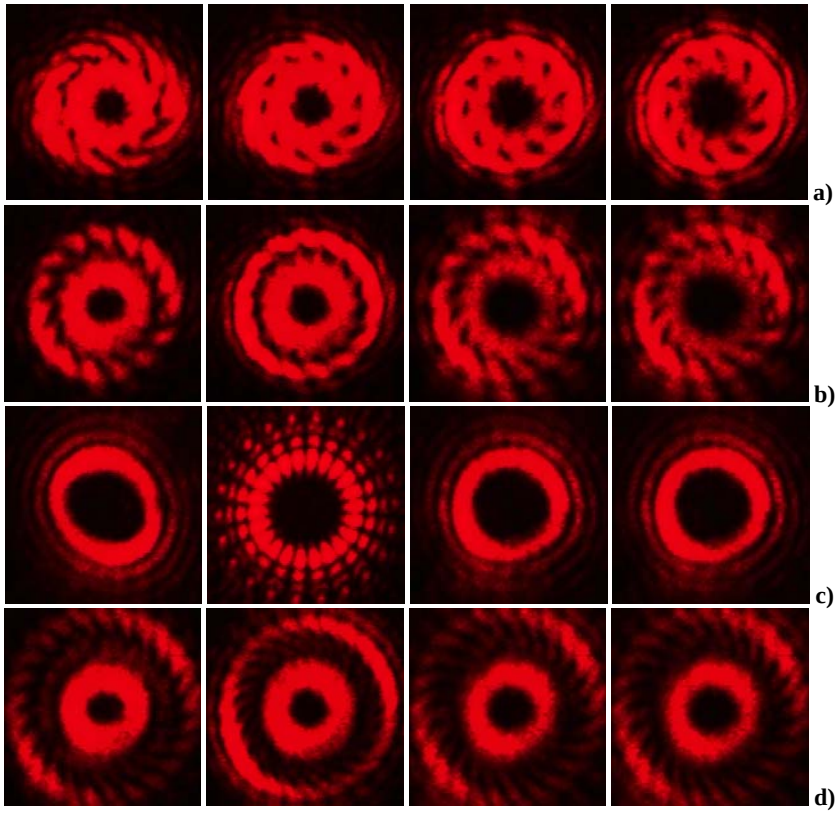

Fig. 10 – a) $m_1 = 5$, $m_2 = 15$; b) $m_1 = 5$, $m_2 = 20$; c) $m_1 = -11$, $m_2 = 11$; d) $m_1 = 5$, m_2=30,
first column $I_2 = 0.001 \cdot I_{ideal}$, second column $I_2 = I_{ideal}$, third column $I_2 = 10^2 \cdot I_{ideal}$, forth column $I_2 = 10^3 \cdot I_{ideal}$.

5. TRANSFERRED INFORMATION

In the free space optical communication based on spatially modulated beams created using optical vortices, an important goal is the identification of each individual OAM state hidden in the DIPs. In the case of axial superposition of two LGBs, one type of the information transferred in the DIPs, has an unhidden character given by the fact that such conditions can be created so that the circular intensity distribution appears as a number of δm maxima and minima visible with a simple radial detection.

Nonetheless, in order to separately read each OAM state, a reading mask must be inserted in the optical path, with the aim to recompose the corresponding Gaussian beam. The reading mask is generated as a phase hologram, which incorporates a spatially-dependent phase retardation, in the 0 to 2π range, in a pattern described by $-m_i\theta$ modulo 2π, where m_i represents one of the OAM initial state.

The case presented in the Fig. 11 is created using two OAM states which fulfill condition 2.1. Figures 11a and 11c display DIPs obtained when in the optical path the suitable reading mask with opposite sign for the OAM was inserted. In Figs. 11b and 11d is presented the case where in the optical path a reading mask generated using a mismatch value for the OAM state was introduced.

Figure 12 presents the cases when the LGBs are generated with OAM states that do not fulfill condition 2.1. In all presented cases, the detection occurs in the central part as a peak, which represents the

recovered Gaussian beam of the read OAM state. The efficiency of the reading process is presented as the ratio between the maximum intensity in this central peak and the maximum intensity outside this central peak (arbitrary units). In Fig. 13 its behavior is presented. In order to obtain an accurate comparison, the same OAM state has been read in all cases.

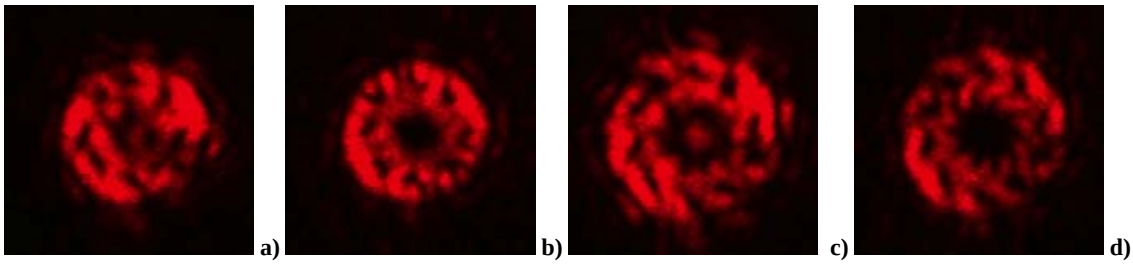

Fig. 11 – Final DIPs generated using DOEs and suitable reading masks in the cases of: a) $m_1 = 3$, $m_2 = 11$ and c) $m_1 = 5$, $m_2=15$; b), d) final DIP generated with mismatching reading mask for the correspondent DOE.

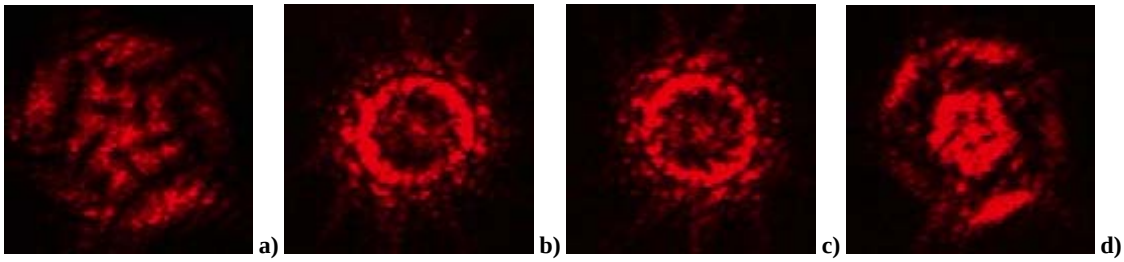

Fig. 12 – Final DIPs generated using DOEs and suitable reading masks in the cases of: a) $m_1 = 5$, $m_2 = 20$; b) $m_1 = 11$, $m_2= –11$ (read 11); c) $m_1 = 11$, $m_2 = –11$ (read –11); d) $m_1 = 5$, $m_2 = 30$.

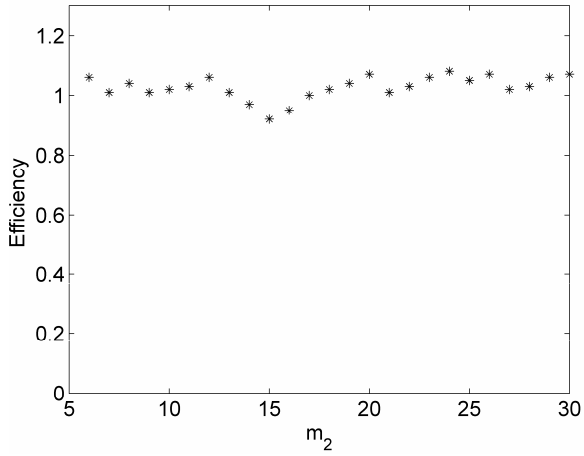

Fig. 13. – Efficiency in the reading process for $m_1 = 5$, when m_2 ranges from 6 to 30.

6. CONCLUSIONS

The diffracted intensity patterns obtained from the superposition of two LGBs were investigated in relation to the constructive parameters values used to separately generate each LGB. The transformation of the intensity spatial distribution goes from constructive interference patterns to separated rings. We showed that different types of DIPs can be obtained by simple changing of the OAM state values at given values for I, w_0 and z: 1) cylindrically symmetric intensity distribution in a lattice with circular holes, 2) cylindrically symmetric intensity distribution with radial petals, and 3) separated concentric bright rings.

The intensity spatial distributions depend on w_0, for all cases of combinations between OAM states, which fulfill or not condition 2.1, for given I and z values. Experimental results show that for z values up to a

few kilometers, the shape of the intensity spatial distribution is invariable. Also, the values for I_2 are not critical in order to fulfill the condition 2.2; values in the range $I_2 \in \left[10^{-3} \cdot I_{ideal},\ 10^{3} \cdot I_{ideal}\right]$ keep stable intensity spatial distribution. We can conclude that the intensity spatial distribution in DIPs have a robust behavior in regard to large intervals for the parameters *I* and *z*.

In the case of the axial superposition of two LGBs, a reading mask inserted in the optical path, recovers the Gaussian shape corresponding to the contained OAM states. For all (1–3) cases of the obtained DIPs, the efficiency in the detection process is comparable.

These observations, regarding DIPs obtained from two LGBs axially superposed propose this combination as a compelling candidate for the optical information transfer, mainly due to the fact that they are robust with respect to the propagation distance and relative intensities. These results will be useful in long-distance optical communications in free-space or turbulent atmosphere.

ACKNOWLEDGMENTS

The research presented in this paper was financed by the contract UEFISCDI, PN-II-PT-PCCA no. 203/2012 from the Romanian Government.

REFERENCES

1. J.E. MORRIS, A.E. CARRUTHERS, M. MAZILU, P.J. REECE, T. CIZMAR, P. FISCHER, K. DHOLAKIA, *Optical micromanipulation using supercontinuum Laguerre-Gaussian and Gaussian beams*, Opt. Expr., **16**, *14*, pp. 10117–10121, 2008.
2. D. COJOC, V. EMILIANI, E. FERRARI, R. MALUREANU, S. CABRINI, R.Z. PROIETTI, E. DI FABRIZIO, *Multiple Optical Trapping by Means of Diffractive Optical Element*s, Jpn. J. Appl. Phys., **43**, pp. 3910–3915, 2004.
3. Z. BOUCHAL, *Nondiffracting optical beams, physical properties, experiments and applications*, Czech. J. Phys., **53**, *7*, pp. 537–578, 2003.
4. S.H. TAO, X.-C. YUAN, B.S. AHLUWALIA, *The generation of an array of nondiffracting beams by a single composite computer generated hologram*, J. Opt. A: Pure Appl. Opt., **7**, pp. 40–46, 2005.
5. J.A. ANGUITA, J.N. HERREROS, I.B. DJORDJEVIC, *Coherent Multimode OAM Superpositions for Multidimensional Modulation*, IEEE Phot. J., **6**, *2*, 7900811, 2014.
6. M. MIHAILESCU, A. SOBETKII, M. PELTEACU, *Two-Steps Profile Diffractive Microlenses Design to Generate Binary Focal Points Along The Propagation Axis*, Rom. J. Inf. Sci. Tech., **13**, *4*, pp. 358–367, 2010.
7. J. THORNES, P. POON, M.E. ANDERSON, *Single-iteration compression of femtosecond laser pulses*, J. Opt. Soc. Am. B, **21**, *7*, pp. 1387–1395, 2004.
8. L. IONEL, *An alternative method for the compensation of laser beam spatial distortions based on computer generated holograms*, Rom. Rep. Phys., **65**, *3*, pp. 984–996, 2013.
9. G. GIBSON, J. COURTIAL, M.J. PADGETT, M. VASNETSOV, V. PASKO, S.M. BARNETT, S. FRANKE-ARNOLD, *Free-space information transfer using light beams carrying orbital angular momentum*, Opt. Expr., **12**, *22*, pp. 5449–5456, 2004.
10. E. SCARLAT, M. MIHAILESCU, A. SOBETKII, *Spatial frequency and fractal complexity in single-to-triple beam*, J. Opt. Adv. Mat., **12**, *1*, pp. 105–109, 2010.
11. A.V. CARPENTIER, H. MICHINEL, J.R. SALGUEIRO, D. OLIVIERI, *Making optical vortices with computer-generated holograms*, Am. J. Phys., **76**, *10*, pp. 916–921, 2008.
12. A. HERMERSCHMIDT, S. KRÜGER, G. WERNICKE, *Binary diffractive beam splitters with arbitrary diffraction angles*, Opt. Lett., **32**, *5*, pp. 448–450, 2007.
13. O. MENDOZA-YERO, M. FERNÁNDEZ-ALONSO, G. MÍNGUEZ-VEGA, J. LANCIS, V. CLIMENT, J. A. MONSORIU, *Fractal generalized zone plates*, J. Opt. Soc. Am. A, **26**, *5*, pp. 1161–1166, 2009.
14. M. CHEN, M. MAZILU, Y. ARITA, E.M. WRIGHT, K. DHOLAKIA, *Dynamics of microparticles trapped in a perfect vortex beam*, Opt. Lett., **38**, *22*, pp. 4919–4922, 2013.
15. S. FRANKE-ARNOLD, J. LEACH, M.J. PADGETT, V.E. LEMBESSIS, D. ELLINAS, A.J. WRIGHT, J.M. GIRKIN, P. OHBERG, A.S. ARNOLD, *Optical ferris wheel for ultracold atoms*, Opt Expr., **15**, *14*, pp. 8619–8625, 2007.
16. J.A. ANGUITA, J. HERREROS, I.B. DJORDJEVIC, *Coherent Multimode OAM Superpositions for Multidimensional Modulation*, IEEE Photonics Journal, **6**, *2*, 7900811, 2014.
17. G. XIE, Y. REN, H. HUANG, N. AHMED, L. LI, Y. YAN, M.P.J. LAVERY, M.J. PADGETT, A.E. WILLNER, *Experimental Analysis of Multiplexing/demultiplexing Laguerre Gaussian Beams with Different Radial Index*, Conference Paper, Frontiers in Optics, Tucson, Arizona United States, October 19–23, 2014.
18. M.J. PADGETT, L. ALLEN, *The Poynting vector in Laguerre-Gaussian laser modes*, Opt. Comm., **121**, pp. 36–40, 1995.

Received May 27, 2015